

DETECTION OF BISTATIC ELECTRON SPIN SIGNALS IN MAGNETIC RESONANCE FORCE MICROSCOPY (MRFM)

Chun-yu Yip*, Alfred O. Hero*, Daniel Rugar†

* University of Michigan, Ann Arbor, MI

† IBM Research Division, Almaden Research Center, San Jose, CA

Abstract

In single spin Magnetic Resonance Force Microscopy (MRFM), the objective is to detect the presence of an electron (or nuclear) spin in a sample volume by measuring spin-induced attonewton forces using a micromachined cantilever. In the OSCAR method of single spin MRFM, the spins are manipulated by an external rf field to produce small periodic deviations in the resonant frequency of the cantilever. These deviations can be detected by frequency demodulation followed by conventional amplitude or energy detection. In this paper, we present an alternative to these detection methods, based on optimal detection theory and Gibbs sampling. On the basis of simulations, we show that our detector outperforms the conventional amplitude and energy detectors for realistic MRFM operating conditions. For example, to achieve a 10% false alarm rate and an 80% correct detection rate our detector has an 8 dB SNR advantage as compared with the conventional amplitude or energy detectors. Furthermore, at these detection rates it comes within 4 dB of the omniscient matched-filter lower bound.

1. INTRODUCTION

Magnetic Resonance Force Microscopy (MRFM) is a recently developed technique with which physicists can potentially push the limits of force detection to the single electron spin level, with sub-angstrom spatial resolution [1–3]. The experiment involves detection of perturbations of a thin micrometer-scale cantilever whose tip incorporates a sub-micron ferromagnet. Any spinning electrons in the sample will act as magnetic dipoles, exerting perturbing forces that can be measured from cantilever displacements. There have been several successful experimental demonstrations of MRFM for imaging micron-size ensembles of spins. For example, three-dimensional imaging with micrometer spatial resolution has been achieved [4]. Furthermore, forces

as small as 8×10^{-19} N have been detected using MRFM [5]. However, despite several advances, detection of an isolated single electron spin has not yet been accomplished. Progress towards this goal will require advances in physical measurements and advances in signal processing of these measurements.

Recently a MRFM method known as Oscillating Cantilever-driven Adiabatic Reversals (OSCAR) [6] has been proposed to detect single spins. This method, explained below, uses a modulated external radio frequency (rf) magnetic field to manipulate the electron spins, in order to produce periodic forces on the cantilever that can be detected as small frequency shifts. Detection of these frequency shifts identifies the presence of the electron spin. If successful, single electron spin detection would be an important step towards the long-term goal of three-dimensional imaging of subsurface atomic structure [7].

Unfortunately, accurate single-spin detection in OSCAR is hampered by several factors. The spin-induced frequency shift signal is extremely weak as a spin induces a frequency shift of only one part in 10^4 . Thus long integration times are required to detect such a signal. However, spin relaxation and decoherence significantly reduce the usable integration time, especially at room temperature. This makes the use of cryogenics (cooling the experimental apparatus down to a fraction of a degree Kelvin) necessary to reduce these effects. However, in this regime the measurements are prone to thermal noise from various sources. Noise and decoherence effects must be taken into account by the detection algorithm in order to achieve the most accurate and reliable single spin detection. Very simple detectors are the baseband “amplitude detector” and “energy detector” which operate on a frequency demodulated version of the cantilever position signal. Such detection schemes are widely used in MRFM, NMR spectroscopy, MRI, and other applications.

In this paper, we present a new approach to baseband detection in OSCAR experiments. The detector is based on a random telegraph model for the baseband signal incorporating Poisson-distributed random spin reversals, random

Research partially supported by DARPA Mosaic program under ARO contract DAAD19-02-C-0055.

initial spin polarity, and Additive White Gaussian Noise (AWGN). In order to accurately decide between the hypotheses of spin absence and presence, we propose a hybrid detection scheme which combines optimal *Bayes* and *General Likelihood Ratio* (GLR) detection principles implemented with Gibbs sampling. Simulations show that our proposed detector can significantly outperform the conventional baseband amplitude and energy detector for realistic post-demodulation signal-to-noise ratios (SNR).

The outline of the paper is as follows. After briefly reviewing the OSCAR experiment in Sec. 2, we describe the proposed signal detection scheme in Sec. 3, and present results of numerical simulations in Sec. 4.

2. DESCRIPTION OF EXPERIMENT

Fig. 1 is a schematic description of the OSCAR experiment. In OSCAR, a submicron ferromagnet is placed at the tip of a cantilever which sits at a distance of approximately 50 nanometers above a sample. In the presence of an applied rf field, electrons in the sample undergo magnetic resonance if the rf field frequency matches the Larmor frequency. Since the Larmor frequency is proportional to the field from the magnetic tip, and because the tip field falls off rapidly with distance, only those spins that are within a thin "resonant slice" just the right distance from the tip will satisfy the condition for magnetic resonance and contribute to the signal. If the cantilever is forced into mechanical oscillation by positive feedback, the tip oscillation induces small shifts in the Larmor frequencies of the spins. Specifically, the tip motion gives rise to an oscillating magnetic field which sweeps the Larmor frequency of the spins in the resonance slice back and forth through resonance. This causes the spin to reverse polarity synchronously with the cantilever motion, and in return, the spin reversals affect the cantilever motion by changing the effective stiffness of the cantilever. When an electron spin is present the spin-cantilever interaction can be detected by measuring small shifts in the period of cantilever oscillation using laser interferometric cantilever position sensing. For more details about OSCAR, see [7–9].

A classical (non-quantum) electro-mechanical description of the spin-cantilever interactions can be developed in the framework adopted by Berman *etal* [10] and Rugar *etal* [11]. We briefly review this framework here. Consider a spin in a rotating frame which rotates at the frequency of the applied rf magnetic field, \mathbf{B}_1 (Fig. 2). The effective magnetic field $\mathbf{B}_{eff}(t)$ in this frame is given by

$$\mathbf{B}_{eff}(t) = B_1 \hat{i} + \Delta B_o(t) \hat{k}, \quad (1)$$

where \hat{i} and \hat{k} are unit vectors in the x and z directions in

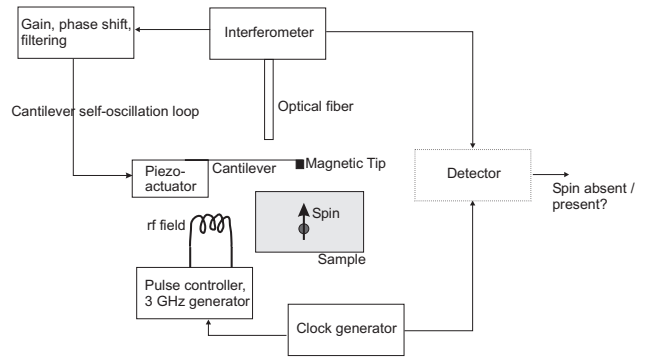


Fig. 1. Schematic of the MRFM experiment.

the rotating frame, B_1 is the amplitude of the rf magnetic field, $B_o(t)$ is the magnetic field caused by the magnetic tip of the cantilever, and $\Delta B_o(t) = B_o(t) - \omega_{rf}/\gamma$ is the off-resonance field magnitude (γ is the gyromagnetic ratio). Spins are in resonance on the spherical shell (resonant slice) defined by those spatial locations for which ω_{rf} matches the Larmor frequency $\gamma B_o(t)$.

If $\Delta B_o(t)$ varies sufficiently slowly such that the adiabatic criterion

$$\frac{d\Delta B_o(t)}{dt} \ll \gamma B_1^2 \quad (2)$$

is met, the spin can be assumed to remain aligned or anti-aligned with the vector $\mathbf{B}_{eff}(t)$. This is the *spin-lock* condition. Let the vertical position of the cantilever tip be denoted by z where $z = 0$ denotes its rest position. Under the influence of the external rf field $\mathbf{B}_1(t)$, electron-spin forces, and random (thermal) force noise $F_n(t)$, the motion of the cantilever tip obeys the simple harmonic oscillator equation:

$$m\ddot{z}(t) + \Gamma\dot{z}(t) + kz(t) = \frac{|\mu|G^2z(t)}{\sqrt{G^2z(t)^2 + B_1^2}} + F_n(t), \quad (3)$$

where m is the cantilever's effective mass, k is the cantilever spring constant, Γ is the friction coefficient characterizing cantilever energy dissipation, $|\mu|$ is the magnitude of the spin magnetic moment, $G = \partial B_{oz}/\partial z$ is the z -direction field gradient at the spin location. The natural mechanical resonance frequency of the cantilever is given by $\omega_o = \sqrt{k/m}$, and Γ can be related to the cantilever quality factor, Q , via $\Gamma = k/(\omega_o Q)$.

Under the small tip displacement approximation $|Gz| \ll B_1$, we obtain

$$m\ddot{z}(t) + \Gamma\dot{z}(t) + (k + \Delta k)z(t) \approx F_n(t), \quad (4)$$

where $\Delta k = -|\mu|G^2/B_1$. This shift in spring constant

results in a shift $\Delta\omega_o$ of the cantilever resonant frequency:

$$\Delta\omega_o \approx -\frac{1}{2}\omega_o \frac{|\boldsymbol{\mu}|G^2}{kB_1}. \quad (5)$$

In a version of the protocol called ‘‘Interrupted OSCAR,’’ the B_1 field is turned off every T_{skip} seconds over a half cycle duration (π/ω_o) to cause periodic transitions between the *spin-lock* and *anti-spin-lock* spin states (see middle panel of Fig. 4). In the spin-lock state the spin aligns with the field $\mathbf{B}_{eff}(t)$ and in the anti-lock state the spin aligns with $-\mathbf{B}_{eff}(t)$. Therefore, the frequency shift $\Delta\omega_o$ of the cantilever alternates between the two values $\pm\frac{1}{2}\omega_o(|\boldsymbol{\mu}|G^2)/(kB_1)$ with period T_{skip} . In the absence of noise ($F_n(t) = 0$ in (3)) the cantilever motion can be expressed as the frequency modulated (FM) signal:

$$z(t) = A \cos\left(\omega_o t + \int_0^t \bar{s}(t') dt' + \theta\right). \quad (6)$$

Here A is the cantilever oscillation amplitude, θ is a random phase, and \bar{s} is equal to 0 if no spin coupling occurs, while it is equal to a periodic square wave of period $2T_{skip}$ and of amplitude $|\Delta\omega_o|$ if spin coupling occurs. Thus, in this ideal noiseless case, the presence of spin coupling can be perfectly detected either by detecting a spectral peak near $|\Delta\omega_o|$ radians in the periodogram or by frequency demodulation of z to baseband (incorporating subtraction of the known center frequency ω_o) followed by amplitude detection, energy detection, or other algorithm, as discussed below. As baseband and narrowband are equivalent representations we focus on the baseband method here. These methods correlate the baseband signal against the known square wave signal derived from B_1 . The resultant signal, which we call $y(t)$, forms the statistic which is used for spin detection, as illustrated in Fig. 3.

Unfortunately, in a practical (non-ideal) experiment the cantilever tip-displacement signal $z(t)$ is degraded by several factors which reduce correlation peak detection accuracy. One factor is the presence of laser interferometric measurement noise. This adds a noise floor to the demodulated square wave signal $\bar{s}(t)$. Another factor is spin relaxation which over a period of time causes the spin to go out of alignment with the effective field \mathbf{B}_{eff} . While several models for single-spin relaxation have been proposed [10, 11], a full understanding of the physics of single-spin relaxation interactions with cantilevers remains open. One model, adopted here, is that the single spins maintain spin lock or anti-lock states but spontaneously and asynchronously change polarity during the course of measurement at some rate λ flips/second. In the sequel we develop an optimal single-spin detection approach under a random Poisson model for these polarity flips.

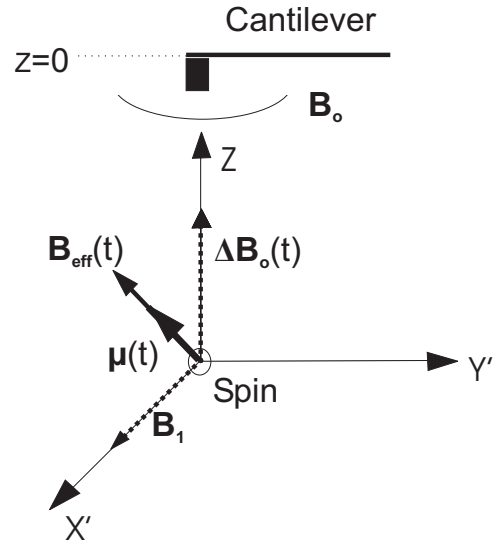


Fig. 2. In the coordinate system rotating at ω_{rf} , the off-resonance field ΔB_o , and therefore the effective field $B_{eff}(t)$, vary with time. Under the spin lock assumption, the spin always follows $\pm B_{eff}(t)$.

3. SIGNAL DETECTION IN NOISE

The signal detectors we will consider operate on the baseband output signal $y(t)$ of the frequency demodulator, e.g. a Phase-Lock Loop (PLL), followed by multiplication by a square wave reference $p(t) \in \{\pm 1\}$ of period $2T_{skip}$, whose transitions are synchronous with the (known) rf turn-off times (see Fig. 3).

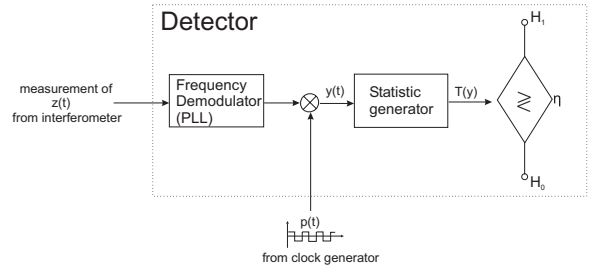


Fig. 3. Baseband detector frequency demodulates the interferometric signal, correlates the output against a square wave $p(t)$ whose transitions are synchronous with the turn-off times of the rf field $B_1(t)$, and generates a test statistic, e.g. accumulated squared frequency deviations, for detecting presence of a spin.

We model the baseband output $y(t)$ of the frequency demodulator and correlator as a random telegraph plus additive Gaussian white noise (see lower panel of Fig. 4). Let $[0, T]$ be the total measurement time period over which the correlator integrates the measurements, and let $\{\tau_i\}$, $i =$

$1..N$, be the time instants within this period at which spin reversals occur. We assume $\{\tau_i\}$ are the arrival times of a Poisson process with intensity λ . Consequently N is a Poisson random variable with rate λT [12]. Thus, $y(t) = s(t) + v(t)$ where $v(t)$ is AWGN with variance $= \sigma_v^2$, and $s(t)$ is a random telegraph signal containing only the random transitions:

$$s(t) = \phi |\Delta\omega_o| \sum_{i=0}^N (-1)^i g\left(\frac{t - \tau_i}{\tau_{i+1} - \tau_i}\right), \quad (7)$$

where ϕ is a random variable that takes on ± 1 with equal probability, representing a random initial spin polarity, $\tau_0 = 0$, $\tau_{N+1} = T$, and $g(t)$ is the standard rectangle function: $g(t) = 1$ for $t \in [0, 1]$ and $g(t) = 0$ otherwise. If there are no random spin flips in the time period $[0, T]$, then $s(t) = \phi |\Delta\omega_o|$ is constant over time, which we obtain in (7) by using the convention that when $N = 0$, $\tau_0 = 0$ and $\tau_1 = \infty$.

The baseband spin detection problem is to design a test between the two hypotheses:

$$\begin{aligned} H_0 \text{ (spin absent): } & y(t) = v(t) \\ H_1 \text{ (spin present): } & y(t) = s(t) + v(t) \end{aligned} \quad (8)$$

for $t \in [0, T]$.

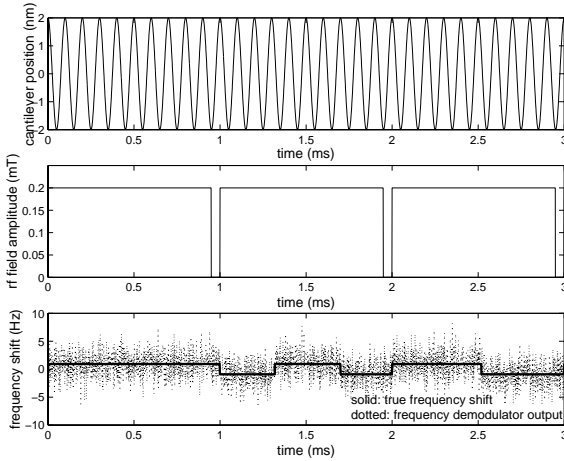


Fig. 4. Top: Sample cantilever position signal, $z(t)$, at 10 kHz. Middle: Sample rf magnetic field magnitude, B_1 , has synchronous half-cycle skips at 1 ms, 2 ms, and 3 ms. Bottom: In the presence of a single spin, \bar{s} in Eq. 6 has both deterministic transitions due to the rf skips at 1 ms, 2 ms and 3 ms, and random ones due to spin relaxation. The random transitions, $\{\tau_i\}$, occur as a Poisson process. The initial polarity is $\phi = 1$ for this example. The noisy signal at bottom is \bar{s} with AWGN contamination.

Conditioned on the random parameters $\{\tau_i\}$, N , ϕ , the signal $s(t)$ is deterministic and known. Under this conditioning the *optimal* detection structure would be the simple

matched filter [13]

$$\frac{1}{T} \int_0^T y(t') s(t', \phi, \tau, N) dt' \underset{H_0}{\overset{H_1}{>}} \eta \quad (9)$$

where $s(t; \phi, \tau, N)$ is a synthesized random telegraph signal of the form (7) parametrized by $|\Delta\omega_o|$ (assumed known), ϕ , τ and N . The value η is a threshold that can either be set to satisfy a *probability of false alarm* (P_F) constraint $P_F \leq \alpha$, $\alpha \in [0, 1]$, or as a function of the prior probabilities $a \ln[P(H_0)/P(H_1)] + b$ where a, b are known constants. In the former case the detector is called the *most powerful* (MP) test of level α , which has maximum *probability of detection* (P_D), while in the latter case the detector is called the minPe detector as it achieves minimum average probability of decision error (minPe).

As the values of the random parameters are always unknown, we call the detector (9) the *omniscient matched filter*, which is unimplementable. However, as the omniscient matched filter is optimal for known parameter values it establishes a useful upper bound on performance.

Perhaps the simplest baseband detection scheme, and the most widespread in MRFM applications, is the *amplitude detector* which acts as if there were no random flips and declares a spin present if the magnitude of the average amplitude of the correlator output exceeds a threshold

$$\left| \frac{1}{T} \int_0^T y(t') dt' \right| \underset{H_0}{\overset{H_1}{>}} \eta \quad (10)$$

where η is a threshold set to give the desired P_F . Improved performance can be obtained by explicitly accounting for the equally likely initial polarity and assuming AWGN to derive the minPe detector. The amplitude detector (10) is the minPe detector under the assumption that $y(t)$ is a random polarity constant embedded in AWGN. This is a valid assumption when there are no random spin flips over the integration period $[0, T]$.

When there are random spin flips over $[0, T]$ due to spin relaxation and decoherence, the performance of the amplitude detector suffers. Indeed, as the number of random flips increases the average amplitude of $y(t)$ converges to zero. As the energy of $s(t)$ is independent of number of transitions, transition times, and initial polarity, it is natural to propose an *energy detector* [13]

$$\int_0^T [y(t')]^2 dt' \underset{H_0}{\overset{H_1}{>}} \eta \quad (11)$$

where η is a threshold set to give the desired P_F . It can be shown that the energy detector is a minPe test for the case that $v(t)$ is additive white gaussian noise, $s(t) =$

$\Delta\omega_o \cos(2\pi t/T_{skip} + \theta)$, and θ is uniformly distributed over $[0, 2\pi]$ [14]. It can also be shown that the energy detector is the minPe test under a Gaussian approximation to the random telegraph process in the limit of high SNR [15]. Note that in our case the detection performance of the energy test is independent of the average flip rate λ .

As we will show in the sequel, the performance of the amplitude and energy detectors can be far from the optimal performance achieved by the omniscient matched filter detector.

3.1. The Hybrid Bayes/GLR Detector

The minPe detector for a signal with random parameters is a Bayes likelihood ratio test that averages an omniscient likelihood ratio test statistic over all random parameters [14]:

$$\begin{aligned} \log \Lambda(y) & \quad (12) \\ &= \log \frac{E_{\tau, N} [E_{\phi} [f(y; \tau, N, \phi | H_1)]]}{f(y | H_0)} \underset{H_0}{\overset{H_1}{>}} \eta. \end{aligned}$$

As above η is a threshold selected to achieve a desired level α of P_F . The function f is the joint p.d.f of $\{y(t)\}_{t \in [0, T]}$ parametrized by the random parameters τ, N, ϕ , and $E_{\mathbf{x}}[\cdot | A]$ denotes conditional expectation over random variables \mathbf{x} given event A .

While the expectation over ϕ in (12) is simple to evaluate, the expectation over $\{\{\tau_i\}, N\}$ is very difficult since the integration region is of very high (infinite) dimension. An alternative to this performing this second expectation is to invoke the Generalized Likelihood Ratio (GLR) principle. The GLR consists of replacing the unknown parameters in (12) by *Maximum Likelihood* (ML) estimates.

$$\begin{aligned} \log \Lambda(y) & \quad (13) \\ &= \log \frac{\max_{\tau, N} \{E_{\phi} [f(y; \tau, N, \phi | H_1)]\}}{f(y | H_0)} \underset{H_0}{\overset{H_1}{>}} \eta, \end{aligned}$$

where, again, η is a threshold chosen for a desired P_F . Note that in (13) we have averaged over ϕ while we have maximized over $\{\{\tau_i\}, N\}$, leading to what we call a hybrid Bayes/GLR test.

As $y(t)$ is a conditionally Gaussian random process given $\{\tau_i\}$ and N , the log-likelihood function in (13) can be simplified by invoking the Cameron-Martin formula [16]:

$$\begin{aligned} \log \Lambda(y) &= \max_{\tau, N} \left\{ \log \cosh \left[\frac{1}{\sigma_v^2} \int_0^T y(t) s^+(t; \tau, N) dt \right] \right\} \\ &\quad - \frac{1}{\sigma_v^2} \int_0^T (s^+(t; \tau, N))^2 dt \end{aligned} \quad (14)$$

where $s^+(t; \tau, N)$ is the synthesized telegraph wave (7) having initial polarity $\phi = 1$ and parameterized by τ and N . It is well known that for a sufficiently large integration time T the minPe and GLR tests are identical (see for example [17]). Thus we can assert that the hybrid Bayes/GLR test (13) is an asymptotically optimal test.

3.2. Solution via Gibbs Sampling

The maximization in (14) by exhaustive search over the uncountably infinite dimensional space of possible parameter values, $\{\{\tau_i\}, N\}$, is impractical. An alternative, which is guaranteed to converge to the maximizing solution, is to more efficiently search over these parameters by Gibbs Sampling [18, 19]. As we know the Poisson intensity λ , we can generate samples $\{\{\tau_i\}, N\}$ from the *prior* Poisson distribution so as to maximize the log-likelihood function. As these samples are more likely (on the average) to mimic the actual behavior of the parameters, we obtain a reduction in search complexity.

The general description of the Gibbs sampler is as follows. Supposed there is a random vector variable $\mathbf{X} = [x_1, x_2, \dots, x_p]^T$ having density function $f_{\mathbf{X}}$ from which we want to sample. Suppose also that we can simulate the i -th element of \mathbf{X} given samples (already simulated) of the other elements:

$$\begin{aligned} & X_i | x_1, x_2, \dots, x_{i-1}, x_{i+1}, \dots, x_p \\ & \sim f_i(x_i | x_1, x_2, \dots, x_{i-1}, x_{i+1}, \dots, x_p) \quad \text{for } i = 1..p \end{aligned} \quad (15)$$

Then a Markov sequence, $\mathbf{x}^{(t)} = [x_1^{(t)}, \dots, x_p^{(t)}]^T$, can be simulated by the recursion

$$\begin{aligned} X_1^{(t+1)} & \sim f_1(x_1 | x_2^{(t)}, \dots, x_p^{(t)}), \\ X_2^{(t+1)} & \sim f_2(x_2 | x_1^{(t+1)}, x_3^{(t)}, \dots, x_p^{(t)}), \\ & \vdots \\ X_p^{(t+1)} & \sim f_p(x_p | x_1^{(t+1)}, x_2^{(t+1)}, \dots, x_{p-1}^{(t+1)}). \end{aligned} \quad (16)$$

After a certain amount of burn-in time T_b , $\mathbf{X}^{(t)}$, $t > T_b$, will have stationary distribution $f_{\mathbf{X}}$. In our case, since the arrival times $\{\tau_i\}$ are generated from a Poisson process, the conditional distributions (16) are easy to sample from, because they are conditionally uniform.

4. SIMULATION METHODS AND RESULTS

The objective of our first three simulations was to compare the detection performance of the matched filter, the am-

plitude detector, the energy detector, and the Bayes/GLR detector on the basis of Receiver Operating Characteristic (ROC) curves, which are obtained by empirically generating the pairs (P_F, P_D) for each detector. In our simulations, the four decision rules (9), (10), (11), and (13) were used to generate the ROC curves in the Matlab 6.1 environment. Based on the Monte Carlo methodology [18], we generated samples $\{y_d^{(i)}(n)\}$, $y_d(n) = y(nT_s)$, under both Hypothesis 0 and 1, where T_s was the sampling period. The samples were input to the detector being evaluated, and P_D and P_F were statistically calculated. 500 detection trials were performed under each hypothesis. For each ROC curve, the above process was repeated with a range of decision threshold values η . This range of thresholds was chosen in order to adequately sample the domain $P_F \in [0, 1]$.

The simulation parameter values were chosen according to typical OSCAR experimental values. The signal duration T was 3 s and the sampling period T_s was 0.5 ms. The rest of the parameters were set to: $k = 1 \times 10^{-3}$ N/m, $\omega_o/(2\pi) = 1 \times 10^4$ Hz, $B_1 = 0.2$ mT, $G = 2 \times 10^6$ T/m, and $\mu = 9.3 \times 10^{-24}$ J/T. With these parameters the (noiseless) signal amplitude, $|s(t)|$, was 0.928 Hz according to (5). Two values of λ , the average number of random flips per second, were evaluated. The detector noise was assumed AWGN and the noise variance was adjusted to investigate the effect of SNR, which is defined as $10 \log_{10}[(1/T) \int_0^T |s(t)|^2 dt / \sigma_v^2]$.

We ran the Gibbs sampler for 5,000 iterations for the hybrid Bayes/GLR detector. Fig. 5 and 6 show ROC curves for SNR = -25 dB and -20 dB, respectively, for $\lambda = 1$ event-per-second. In both cases, our hybrid Bayes/GLR detector significantly outperformed all the other detectors except for the unimplementable matched filter. The matched filter had complete information about the random flip times, and as a result it achieved almost perfect detection for both SNR values. In Fig. 7 the value of λ was increased to 10 events-per-second and the SNR was held at -20 dB. As expected, the performance of the amplitude and hybrid Bayes/GLR detectors degrades, while the matched filter and energy detector, whose performance does not depend on λ , are not affected. In Fig. 8 the power curves for all detectors are plotted as a function of SNR for $\lambda = 1$. Here all detectors perform at the same false alarm rate $P_F = 0.1$, and we can make a quantitative SNR comparison by fixing the detection performance level at $P_D = 0.8$, say. To attain this detection level, the energy detector and amplitude detector require SNR's of at least -14 dB and -17.5 dB, respectively, while the hybrid Bayes/GLR detector only requires -26 dB. As compared to the amplitude detector, this represents an improvement of almost 9 dB in SNR performance using our proposed detector. Furthermore, the performance of our proposed detector is only 4 dB worse than the performance bound of -30 dB

established by the matched filter for this level of P_F and P_D . Note that the amplitude detector outperforms the energy detector for low SNR's but not for high SNR's. This is explained by the fact that even though the energy detector is not affected by random flips, at low SNR's its test statistic is dominated by the noise.

In another simulation, we investigated the role of the number of Gibbs samples on performance of the hybrid Bayes/GLR detector, shown in Fig. 9. It is evident that performance improves as we increase the number of Gibbs samples. For example, at $P_F = 0.1$, P_D increases from approximately 0.35 to 0.65 if we increase the number of Gibbs samples from 100 to 500. It increases further to around 0.9 and 0.95 if 500 or 5,000 Gibbs samples are used, respectively. Such improvements in performance are significant but yield diminishing returns as the number of Gibbs samples is increased beyond 500.

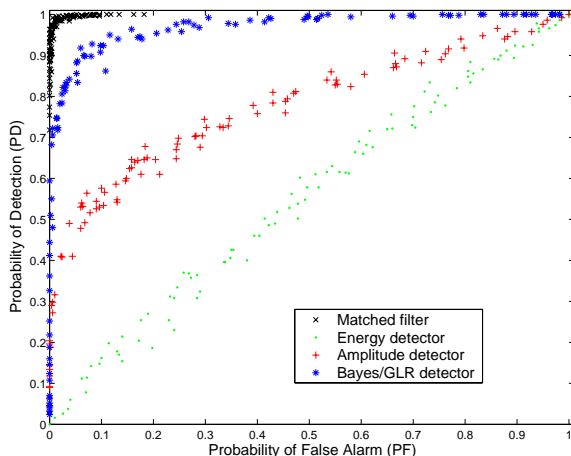


Fig. 5. Simulated Receiver Operating Characteristic (ROC) curves for the matched filter, energy detector, amplitude detector, and hybrid Bayes/GLR detector, at SNR = -25 dB and $\lambda = 1$ event-per-second. Unlike the other detectors, the matched filter assumes complete information on the parameter values and is not implementable.

5. CONCLUSION

In this paper we presented a hybrid Bayes/GLR approach to detecting the presence of single spins for the OSCAR MRFM experiment. We have shown by simulation that the Bayes/GLR detector performs significantly better than the classical amplitude and energy detectors. The improvement in detection performance is due to the fact that, unlike the classical detectors, the new detector estimates the unknown values of the random spin reversal times and the initial polarity. Of course this performance improvement comes at

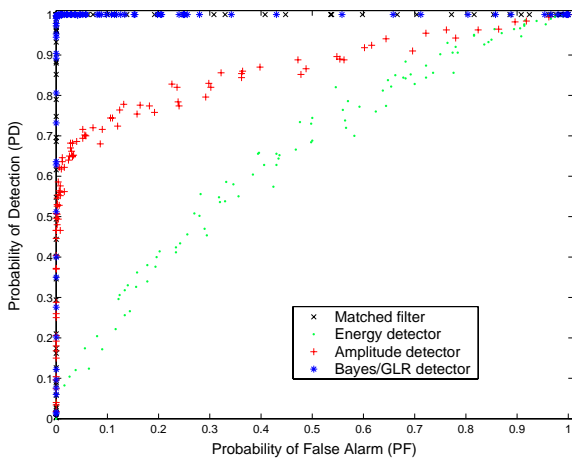


Fig. 6. Simulated Receiver Operating Characteristic (ROC) curves for the matched filter, energy detector, amplitude detector, and hybrid Bayes/GLR detector, at SNR = -20 dB and $\lambda = 1$ event-per-second.

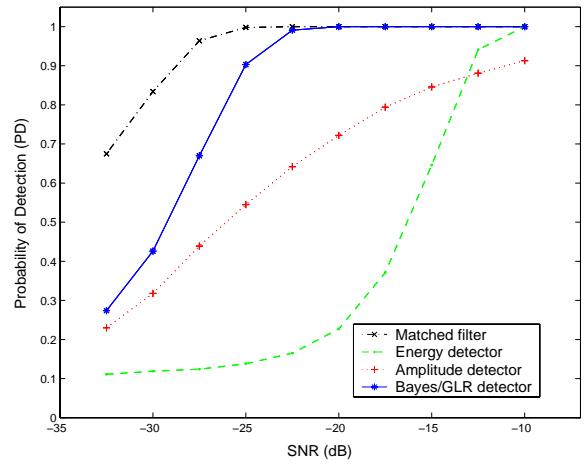


Fig. 8. The power curves (P_D vs. SNR) for the four detectors studied in this paper for $P_F = 0.1$ and $\lambda = 1$ event-per-second. At $P_D = 0.8$ the hybrid Bayes/GLR detector performs within 4 dB of the bound established by the matched filter.

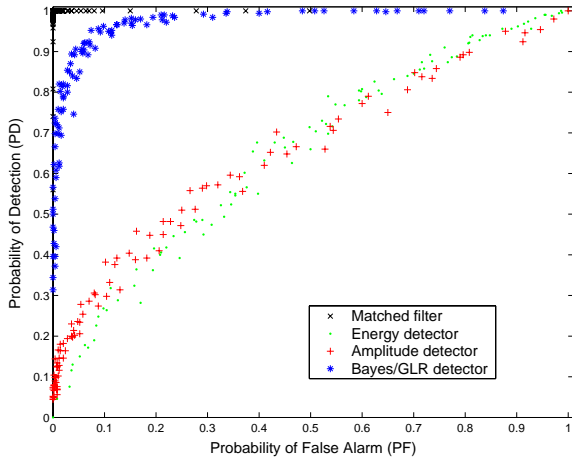


Fig. 7. Simulated Receiver Operating Characteristic (ROC) curves for the matched filter, energy detector, amplitude detector, and hybrid Bayes/GLR detector, at SNR = -20 dB and $\lambda = 10$ events-per-second.

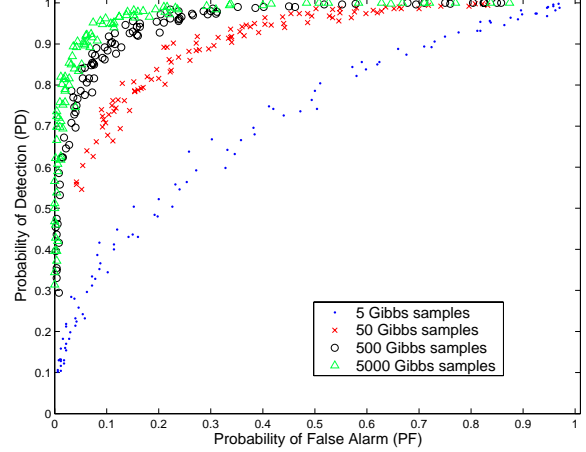


Fig. 9. Juxtaposition of ROC curves of hybrid Bayes/GLR detector, obtained with different numbers of Gibbs samples in the maximization step, at SNR = -20 dB and $\lambda = 10$ events-per-second. Performance improves as the number of Gibbs samples increases.

the price of increased implementation complexity. This complexity increases in the random reversal rate λ due to the necessity to perform Gibbs sampling over an increasingly large number of probable spin reversal sequences. Nonetheless, for the experiments in the first simulation with $\lambda = 1$ event-per-second, the run time of our detector (5,000 Gibbs samples) was only on the order of about half a minute per 3-second measurement record (our code was implemented in Matlab 6.5, under WindowsXP on a 2.26GHz PC, with 510MB RAM).

An interesting extension of our results would be to assume that the frequency shift $|\Delta\omega_o|$ is also unknown. This would lead to a hybrid Bayes/GLR detector which detects the peak over the spectrum of the signal in addition to maximizing over the number and positions of the transitions.

The hybrid Bayes/GLR detector was derived using a baseband signal model consisting of a random telegraph wave with Poisson transitions and AWGN. This signal model is theoretically justified under the spin-lock assumption. The validity of the spin-lock assumption remains to

be established. More sophisticated signal models of the cantilever measurements, and associated detection methods which bypass frequency demodulation and operate directly on those measurements, are currently under investigation.

6. REFERENCES

- [1] J. A. Sidles. Nondestructive detection of single-proton magnetic resonance. *Appl. Phys. Lett.*, 58:2854–2856, 1991.
- [2] J. A. Sidles, J. L. Garbini, and G. P. Drobny. The theory of oscillator-coupled magnetic resonance with potential applications to molecular imaging. *Rev. Sci. Instrum.*, 63:3881–3899, 1992.
- [3] D. Rugar, B. C. Stipe, H. J. Mamin, C. S. Yannoni, T. D. Stowe, K. Y. Yasumura, and T. W. Kenny. Adventures in attonewton force detection. *Appl. Phys. A*, 72[Suppl.]:S3–S20, 2001.
- [4] O. Züger, S. T. Heon, C. S. Yannoni, and D. Rugar. Three-dimensional imaging with a nuclear magnetic resonance force microscope. *J. Appl. Phys.*, 79(4):1881–1884, 1996.
- [5] H. J. Mamin and D. Rugar. Sub-attonewton force detection at millikelvin temperatures. *Appl. Phys. A*, 79:3358, 2001.
- [6] B. C. Stipe, H. J. Mamin, C. S. Yannoni, T. D. Stowe, T. W. Kenny, and D. Rugar. Electron spin relaxation near a micron-size ferromagnet. *Phys. Rev. Lett.*, 8727(27):0502+, 2001.
- [7] J. A. Sidles, J. L. Garbini, K. J. Bruland, D. Rugar, O. Züger, S. Hoen, and C. S. Yannoni. Magnetic resonance force microscopy. *Rev. of Modern Phys.*, 67(1):249–265, 1995.
- [8] D. Rugar, O. Züger, S. T. Hoen, C. S. Yannoni, H. M. Vieth, and R. Kendrick. Force detection of nuclear magnetic resonance. *Science*, 264:1560, 1994.
- [9] K. Wago, D. Botkin, C. S. Yannoni, and D. Rugar. Force-detected electron-spin resonance: Adiabatic inversion, nutation, and spin echo. *Phys. Rev. B*, 57(2):1108–1114, 1998.
- [10] G. P. Berman, D. I. Kamenev, and V. I. Tsifrinovich. Stationary cantilever vibrations in the oscillating cantilever-driven adiabatic reversals - magnetic resonance force microscopy technique. *Quant. Phys.*, March, 2002.
- [11] D. Rugar and R. Budakian. Classical dynamics of a spin interacting with a MRFM cantilever. Technical report, IBM, Almaden Research Center, July 11 2002.
- [12] W. B. Davenport. *Probability and Random Process*. McGraw-Hill, New York, NY, 1970.
- [13] H. V. Poor. *An Introduction to Signal Detection and Estimation*. Springer-Verlag, New York, NY, 1988.
- [14] H. L. Van Trees. *Detection, Estimation, and Modulation Theory (Part I)*. Wiley, New York, NY, 1968.
- [15] A. Hero, M. Ting, C. Y. Yip, and Cyrille Hory. Optimal strategies for single spin detection in MRFM. *in preparation*, 2003.
- [16] L. M. Garth and H. V. Poor. Detection of non-gaussian signals: A paradigm for modern statistical signal processing. *IEEE Proceedings*, 82(7):1061–1095, 1994.
- [17] L. LeCam. *Asymptotic Methods in Statistical Decision theory*. Springer-Verlag, New York, NY, 1986.
- [18] C. P. Robert and G. Casella. *Monte Carlo Statistical Methods*. Springer-Verlag, New York, NY, 1999.
- [19] P. Brémaud. *Markov Chains - Gibbs fields, Monte Carlo Simulation, and Queues*. Springer-Verlag, New York, NY, 1999.